Effective Resistance of Finite Two-Dimensional Grids Based on Infinity Mirror Technique

Rassul Bairamkulov, *Student Member, IEEE*, and Eby G. Friedman, *Fellow, IEEE*

***Abstract*— Conventional numerical circuit analysis tools typically scale superlinearly with the number of nodes. With the rapid increase in nodes in modern VLSI systems, alternative methods are required. The effective resistance is an important characteristic of electrical systems, which is used to simplify the circuit analysis process. An infinite resistive rectangular mesh is commonly assumed in the analysis of grid structures to determine the effective resistance of a grid. The assumption of infinity provides a useful approximation when a large grid is analyzed far from the boundaries. If however the grid is analyzed in close proximity to a boundary or if the grid dimensions are small, the assumption of infinity may lead to significant error. To address this issue, the infinity mirror technique is proposed to determine the effective resistance of a two-dimensional structure, where one or both dimensions are finite. The method exhibits good agreement with nodal analysis, achieving an error below 1% in case studies. The proposed expressions enhance the speed of static grid analysis by several orders of magnitude by replacing computationally expensive nodal analysis with an equivalent reduced grid analysis. A 1,400 fold speedup is achieved in the analysis of 100 nodes within a $10^3 \times 10^4$ grid.**

***Index Terms*— Very large scale integration (VLSI), circuit analysis, circuit simulation, resistance, equivalent circuits, passive circuits, graph theory, functional analysis, power distribution, power dissipation.**

I. Introduction

A RECTANGULAR mesh is a common structure in science and engineering. In engineering, a rectangular mesh is used to model on-chip power and ground networks and silicon substrates, as well as electrically and thermally conductive media. Applications specific to very large scale integration (VLSI) circuits include digital logic, memory, and power and ground distribution networks [1]. In modern VLSI systems, large grid sizes are common. Conventional numerical analysis techniques to solve a large system of linear equations result in prohibitive computational time.

The effective resistance is an important characteristic of these grid structures. Applications include static power and ground network analysis [2], [3], decoupling capacitor allocation [4], [5], RC delay optimization [6], electrically and thermally conductive media [7], [8], and certain graph characteristics, such as coverage and commute times [9]. From the perspective of circuit analysis, the effective resistance can be utilized to significantly reduce the computational complexity of the grid analysis process [2].

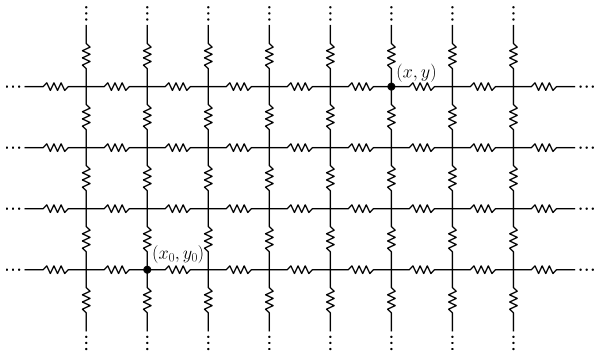

Fig. 1. Infinite two-dimensional grid.

The effective resistance of an infinite resistive lattice is a classical problem in circuit theory [10]. The objective is to determine an equivalent resistance between two arbitrary points within an infinite two-dimensional grid of resistors. The effective resistance between two adjacent points within a two-dimensional isotropic mesh has been determined using symmetry and superposition [11]. In the case of non-adjacent nodes, however, more advanced methods are required. At least six different solutions have been developed since 1940 for this problem, such as random walk theory [12], elliptic integrals [13], Fourier transforms [14]–[16] and Green's function [17]. The problem has been extended to a variety of infinite structures, such as hypercubes [15], [17], [18], triangles [15], [17], hexagons [15], [17], tori and cylinders [19], and anisotropic rectangular lattices [20].

Expressions describing an infinite grid exhibit good agreement with nodal analysis if the effective resistance is measured between nodes located far from the boundary of the grid. Prohibitively large error can however be produced when the resistance is measured between nodes located close to the grid boundaries [21]. Despite the well studied nature of this problem, less attention has been devoted to the analysis of truncated and finite rectangular grids.

Different finite regular structures have been investigated in the literature, including generalized linear chains [22] and circulant graphs [23]. Truncation along one and two dimensions

Manuscript received August 29, 2019; revised January 8, 2020 and March 10, 2020; accepted March 18, 2020. Date of publication April 24, 2020; date of current version September 2, 2020. This work was supported in part by the National Science Foundation under Grant CCF-1526466 and Grant CCF-1716091, in part by IARPA under Grant W911NF-17-9-0001, and in part by grants from Cisco Systems, Qualcomm, and Synopsys. This article was recommended by Associate Editor E. Tlelo-Cuautle. *(Corresponding author: Rassul Bairamkulov.)*

The authors are with the Department of Electrical and Computer Engineering, University of Rochester, Rochester, NY 14627 USA (e-mail: rbairamk@ur.rochester.edu; friedman@ece.rochester.edu).

Color versions of one or more of the figures in this article are available online at http://ieeexplore.ieee.org.

Digital Object Identifier 10.1109/TCSI.2020.2985652

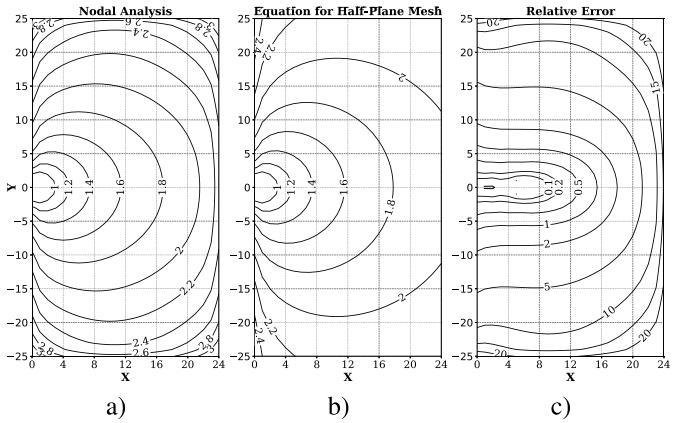

Fig. 2. Effective resistance and relative error of a 25×51 isotropic grid between node $(0, 0)$ and (x, y). a) Evaluation using nodal analysis, b) evaluation using the half-plane mesh equation [21], and c) error (in per cent) of (b) relative to (a).

has been analyzed in previous work using the circuit-level image technique [21]. While the expressions described in [21] are in good agreement with nodal analysis if the resistance is within close proximity of a single boundary or corner, these expressions become inaccurate if the resistance is measured between terminals located at opposite boundaries and corners. The double-sum expressions for the effective resistance in the various grid structures have previously been described in [24]. The computational complexity of these expressions, however, increases linearly with the number of nodes. In this paper, the infinity mirror technique extends the image method to finite structures. With this technique, the effective resistance is determined with high accuracy in a finite rectangular grid of arbitrary size with potential extension to cubic and hypercubic topologies. The computational complexity of the proposed expressions does not depend on the grid size and number of nodes.

To illustrate the relevance of the infinity mirror technique, consider a 25×51 uniform resistive grid. The effective resistance is determined between the node on the left boundary and all other nodes using nodal analysis (Fig. 2a) and the half-plane mesh equation (Fig. 2b) [21]. The relative error is shown in Fig. 2c. While the error is low close to the left boundary, the error may exceed 15% if the half-plane equation is used to evaluate the resistance at the opposite boundary of the grid.

This paper is organized as follows. In section II, the infinity mirror technique is reviewed, which extends the image method described in [21] to finite structures. The effective resistance in grids with finite dimensions is also presented. In section III, these expressions are modified to enhance the efficiency while maintaining accuracy below 1%. Application of the infinity mirror technique to practical problems is presented in section IV using three case studies. Computational speedup of up to five orders of magnitude is demonstrated for certain scenarios. Summary comments are provided in section V.

II. Infinity Mirror Technique

The effective resistance between two points within a mesh is determined using the method adapted from [14]. Consider a two-dimensional resistive mesh. Pick two nodes, (x_0, y_0) and (x, y), at a finite distance between each other with ground infinitely far. Connect the current source injecting current I into (x_0, y_0). The resulting potential at (x_0, y_0) and (x, y) due to the current source at (x_0, y_0) is, respectively, $\phi^{x_0,y_0}(x_0, y_0)$ and $\phi^{x_0,y_0}(x, y)$. Remove the current source at (x_0, y_0) and inject current $-I$ into (x, y). The resulting potential at (x_0, y_0) and (x, y) is, respectively, $-\phi^{x,y}(x_0, y_0)$ and $-\phi^{x,y}(x, y)$. The effective resistance can be determined by superimposing these solutions,

$$R_{eff} = \frac{V(x_0, y_0) - V(x, y)}{I}, \tag{1}$$

where $V(x_0, y_0)$ and $V(x, y)$ are the effective voltage at, respectively, (x_0, y_0) and (x, y) due to all current sources within the grid. $V(x_0, y_0)$ and $V(x, y)$ can be expressed, respectively, as the superposition of potentials due to each individual current source,

$$V(x_0, y_0) = \phi^{x_0,y_0}(x_0, y_0) - \phi^{x,y}(x_0, y_0), \tag{2}$$

$$V(x, y) = \phi^{x_0,y_0}(x, y) - \phi^{x,y}(x, y). \tag{3}$$

The problem of determining the effective resistance within a grid reduces to finding the electric potential caused by the injected current. A similar approach is applicable to truncated grids. As in the case of a fully infinite mesh, the effective resistance in a truncated mesh structure is determined from (1). The voltages, $V(x_0, y_0)$ and $V(x, y)$, however, change to consider the effects of the boundaries modeled as image current sources.

The image method for an infinite grid was introduced in [21] and applied to half- and quarter-plane mesh structures. The resulting effective resistance expressions exhibit good agreement with the resistance of a large grid near a boundary or a corner, where the effects of opposite boundaries can be neglected. If however the effects of the opposite boundaries are significant; for example, if the effective resistance is measured between the opposite corners of a finite rectangular mesh, these expressions are no longer accurate. Efficient methods for determining the effective resistance in a grid where at least one dimension is finite are presented in this section. In subsection II-A, an expression is presented for an infinite strip, a mesh which is finite in one dimension and unbounded in another dimension ($y \in \mathbb{Z}$). This result is utilized in subsection II-B to determine the effective resistance within a semi-infinite strip, an infinite strip truncated along the infinite dimension ($y \in \mathbb{N}_0$). An expression for a finite mesh is presented in subsection II-C. Generalization of the method to higher dimensions is provided in subsection II-D

A. Infinite Strip

Consider the circuit shown in Fig. 3a, where a resistive grid is bounded between 0 and $(w_x - 1)$ in the x-dimension and is unbounded in the y-dimension. The number of nodes in a row along the x-dimension is w_x and is described here as the width of the grid. The bounds of the strip obstruct the current from flowing between the node pairs, $\{(-1, y), (0, y)\}$ and $\{(w_x - 1, y), (w_x, y)\}$.

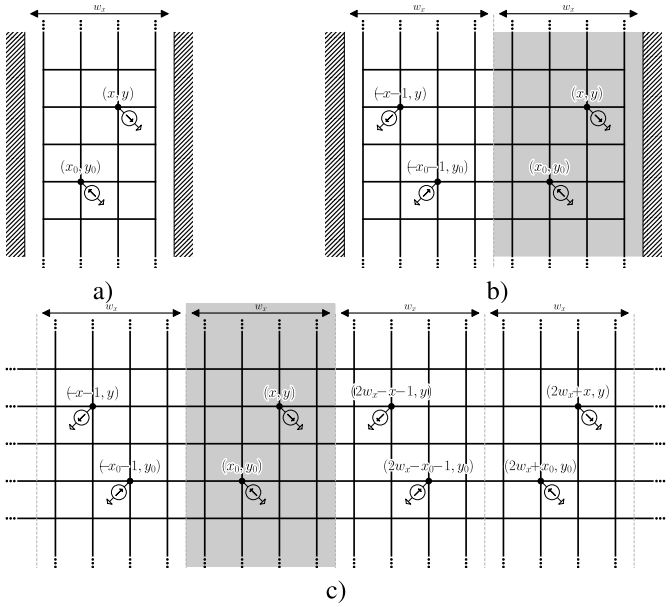

Fig. 3. Infinity mirror method applied to an infinite resistive strip of width w_x. a) Original resistive strip, b) first iteration of image method, and c) infinity mirror technique. In each case, the potential distribution is preserved for $0 \le x \le w_x$.

To provide a solution for an infinite strip, symmetry needs to be restored. Following the approach outlined in [21], the current through the $\{(-1, y), (0, y)\}$ resistor within an infinite resistive grid can be eliminated by applying the image of the strip, as shown in Fig. 3b. The image current sources produce a symmetric potential within the strip that equalizes the potential at $(-1, y)$ and $(0, y)$, resulting in zero current flowing between the pair of nodes. The width of the strip is therefore doubled, while maintaining the potential distribution within the strip. By iteratively repeating the image process for the left and right boundaries, the topology shown in Fig. 3c is produced. Intuitively, the topology is similar to placing an object between two parallel mirrors, leading to infinite images of the object.

The resulting voltage at (x_0, y_0) and (x, y) can be described, respectively, as

$$V_{x_0,y_0} = \sum_{i\in\mathbb{Z}} \big(\phi_{i0}(0,0) + \phi_{i0}(2x_0+1,0) - \phi_{i0}(x-x_0, y-y_0) - \phi_{i0}(x+x_0+1, y-y_0)\big), \tag{4}$$

$$V_{x,y} = \sum_{i\in\mathbb{Z}} \big(-\phi_{i0}(0,0) - \phi_{i0}(2x+1,0) + \phi_{i0}(x-x_0, y-y_0) + \phi_{i0}(x+x_0+1, y-y_0)\big), \tag{5}$$

where $\phi_{ij}(x, y) \equiv \phi(x + 2i w_x, y + 2j w_y)$. The effective resistance is determined from the difference between the voltage at (x_0, y_0) and (x, y),

$$R_{w_x,\infty} I = \sum_{i\in\mathbb{Z}} \big(2\phi_{i0}(0,0) + \phi_{i0}(2x_0+1,0) + \phi_{i0}(2x+1,0) - 2\phi_{i0}(x-x_0, y-y_0) - 2\phi_{i0}(x+x_0+1, y-y_0)\big). \tag{6}$$

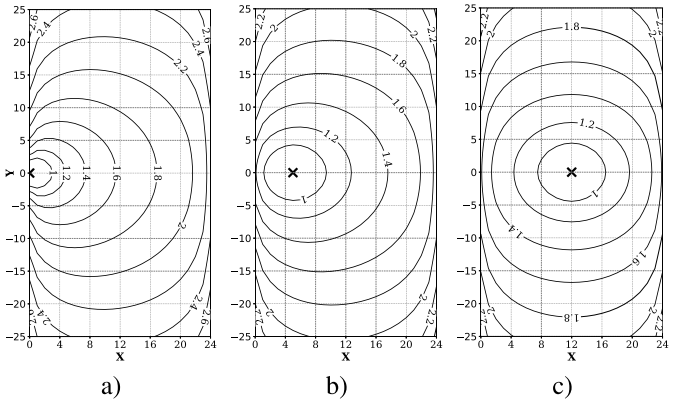

Fig. 4. Effective resistance of an infinite strip of width $w_x = 25$ between point (x_0, y_0) and (x, y) for $k = 1$, a) $x_0 = y_0 = 0$, b) $x_0 = y_0 = 5$, and c) $x_0 = y_0 = 12$. The point (x_0, y_0) is indicated by an $\times$.

From the effective resistance of a fully infinite mesh [21],

$$\frac{R_{w_x,\infty}}{r} = \sum_{i\in\mathbb{Z}} \big(2\Omega^k_{i0}(x-x_0, y-y_0) + 2\Omega^k_{i0}(x+x_0+1, y-y_0) - 2\Omega^k_{i0}(0,0) - \Omega^k_{i0}(2x_0+1,0) - \Omega^k_{i0}(2x+1,0), \tag{7}$$

where r and kr are the resistance of a single resistor in, respectively, the x- and y-dimensions, and

$$\Omega^k_{ij} \equiv \Omega^k(x + 2i w_x, y + 2j w_y) \tag{8}$$

$$\Omega^k(x, y) \equiv \frac{k}{2\pi}\int_0^\pi \frac{1 - e^{-|x|\alpha}\cos(y\beta)}{\sinh(\alpha)} d\beta, \tag{9}$$

$$\alpha = \cosh^{-1}(1 + k - k\cos(\beta)). \tag{10}$$

The contour of (7) is shown in Fig. 4. Note that the effective resistance increases close to the boundaries of the strip, similar to the half- and quarter-plane meshes [21] due to the limited accessibility of the nodes near the boundaries. This behavior is consistent with the Monotonicity Law where the effective resistance increases with the removal of branches [18], [25]. Also note that the effective resistance evaluated from the middle of the strip ($x_0 = \frac{w_x-1}{2}$ for $w_x = 2n + 1, n \in \mathbb{N}_0$) is symmetric with respect to $x = x_0$ and $y = y_0$ (see Fig. 4c).

B. Semi-Infinite Strip

Consider the case where the infinite strip is truncated, bounding the strip between 0 and infinity along the y-dimension. The effective resistance in this case is determined by applying an image of the infinite strip along $x = 0$, as shown in Fig. 5.

$$\frac{R_{w_x,\infty/2}}{r} = \sum_{n\in\mathbb{Z}} \big(2\Omega^k_{i0}(x-x_0, y-y_0) + 2\Omega^k_{i0} \times (x+x_0+1, y+y_0+1) + 2\Omega^k_{i0} \times (x-x_0, y+y_0+1) + 2\Omega^k_{i0}(x+x_0+1, y-y_0) - 2\Omega^k_{i0}(0,0) - \Omega^k_{i0}(2x_0+1,0) - \Omega^k_{i0}(2x+1,0) - \Omega^k_{i0}(0, 2y_0+1) - \Omega^k_{i0}(0, 2y+1) - \Omega^k_{i0}(2x_0+1, 2y_0+1) - \Omega^k_{i0}(2x+1, 2y+1)\big). \tag{11}$$

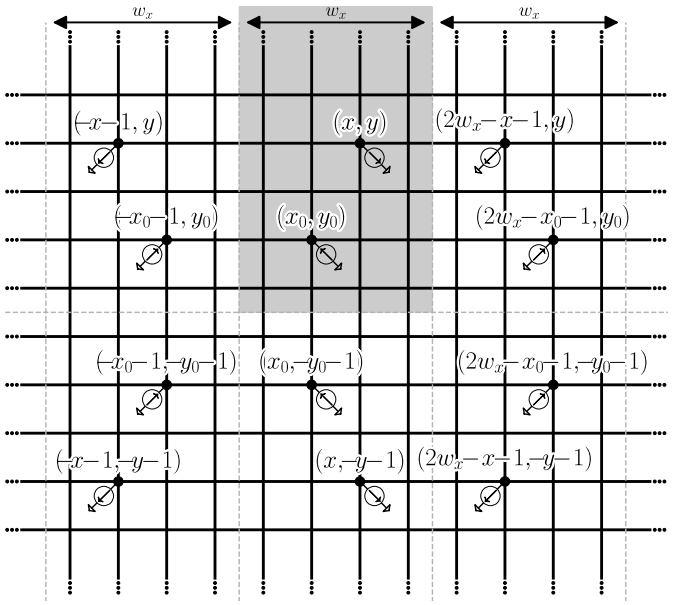

Fig. 5. Infinity mirror technique applied to a semi-infinite resistive strip of width w_x. The original semi-infinite strip is shaded. The potential distribution is preserved for $0 \le x \le w_x$ and $y \in \mathbb{N}_0$.

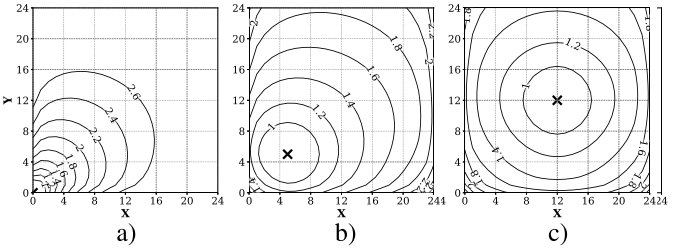

Fig. 6. Effective resistance of a semi-infinite strip of width $wx = 25$ between point (x_0, y_0) and (x, y) for $k = 1$, a) $x_0 = y_0 = 0$, b) $x_0 = y_0 = 5$, and c) $x_0 = y_0 = 12$. The point (x_0, y_0) is indicated by an $\times$.

A contour of (11) is shown in Fig. 6. As compared to Fig. 4, the effective resistance increases at a higher rate, particularly in the x-direction due to the truncation at $y = 0$. Note that the effective resistance evaluated at the middle of the semi-infinite strip is symmetric along the x-dimension, similar to the infinite strip.

C. Finite Mesh

Consider the case where a semi-infinite strip is truncated at $y = w_y - 1$, resulting in a $w_x \times w_y$ finite mesh. The effective resistance can be determined by applying the infinity mirror technique in two dimensions, as shown in Fig. 7. This topology can be modeled using the infinite mirror technique twice, along the x- and y-directions,

$$\begin{aligned} R_{w_x,w_y} = \sum_{i\in\mathbb{Z}} \sum_{j\in\mathbb{Z}} \big(& 2\Omega_{ij}^k(x - x_0, y - y_0) \\ & + 2\Omega_{ij}^k(x - x_0, y + y_0 + 1) \\ & + 2\Omega_{ij}^k(x + x_0 + 1, y + y_0 + 1) \\ & + 2\Omega_{ij}^k(x + x_0 + 1, y - y_0) \end{aligned}$$

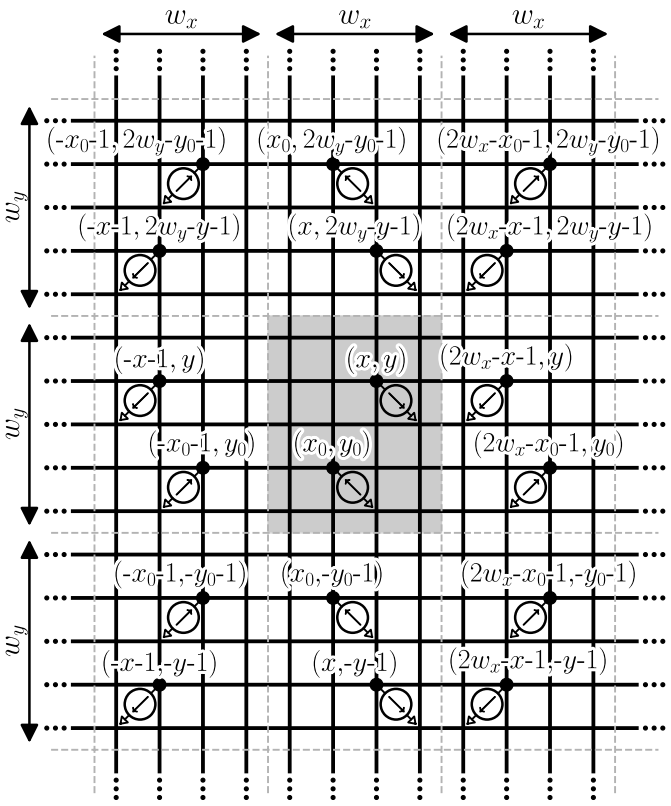

Fig. 7. Infinity mirror technique applied to a finite $w_x \times w_y$ resistive mesh. The original mesh is shaded. The potential distribution is preserved for $0 \le x \le w_x$ and $0 \le y \le w_y$.

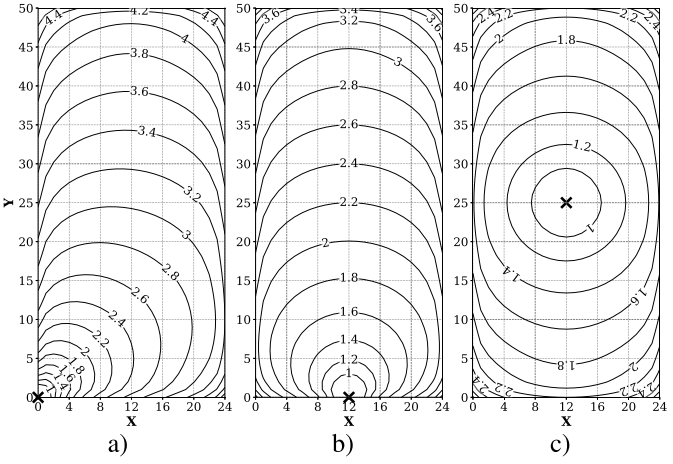

Fig. 8. Effective resistance of a finite grid between (x_0, y_0) and (x, y) within a 25×51 grid for $k = 1$, a) $x_0 = y_0 = 0$, b) $x_0 = 0$, $y_0 = 12$, and c) $x_0 = 12$, $y_0 = 25$. The point (x_0, y_0) is indicated with an $\times$.

$$\begin{aligned} & - \Omega_{ij}^k(2x_0 + 1, 0) - \Omega_{ij}^k(2x_0 + 1, 2y_0 + 1) \\ & - \Omega_{ij}^k(0, 2y_0 + 1)) - \Omega_{ij}^k(2x + 1, 0) \\ & - \Omega_{ij}^k(2x + 1, 2y + 1) - \Omega_{ij}^k(0, 2y + 1) \\ & - 2\Omega_{ij}^k(0, 0)\big). \end{aligned} \tag{12}$$

The resulting resistance in a 25×51 grid is shown in Fig. 8. Several important features can be observed. Note that in the y-direction, the effective resistance increases at a higher rate as compared to the infinite and semi-infinite strips due to the

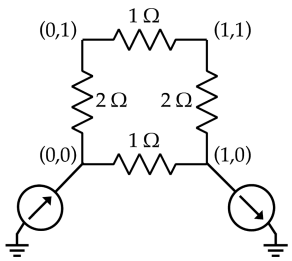

Fig. 9. 2×2 resistive grid. The resistance is measured between nodes $(0, 0)$ and $(1, 0)$

TABLE I
SUMMANDS OF (12) FOR $(x_0, y_0) = (0, 0)$ AND $(x, y) = (0, 1)$ IN A 2×2 RESISTIVE GRID

n \ k	-3	-2	-1	0	1	2	3
-3	0.000	0.000	0.000	0.000	0.000	0.000	0.000
-2	0.000	0.000	0.001	0.000	-0.001	-0.001	0.000
-1	0.000	0.000	0.003	0.004	-0.005	-0.001	0.000
0	-0.001	-0.002	-0.013	0.794	0.044	0.005	0.001
1	0.000	0.000	0.003	0.010	-0.009	-0.001	0.000
2	0.000	0.001	0.001	0.000	-0.001	-0.001	0.000
3	0.000	0.000	0.000	0.000	0.000	0.000	0.000

contribution of the image sources in y-dimension. Also note that a uniform grid exhibits a high degree of symmetry.

To illustrate the infinity mirror technique on a practical circuit, consider the extreme case of the 2×2 nonuniform resistive network shown in Fig. 9. The effective resistance between nodes $(0, 0)$ and $(1, 0)$ is, by Ohm's law, 0.833 ohms. Iteratively evaluating the summands of (12) around $n = k = 0$ efficiently converges to the actual resistance, as listed in Table I. Note that the summands of $|n|, |k| \geq 3$ do not exceed 0.001, indicating that only a small number of images around the origin needs to be considered.

D. Generalization to Higher Dimensions

The proposed technique can be extended to higher dimensions to evaluate the resistance of a multidimensional finite grid. Consider an n-dimensional finite grid with dimensions $\mathbf{w} = [w_1, w_2, \ldots, w_n]$. The resistance is evaluated between source node $\mathbf{x}_s = \left[x_s^1, x_s^2, \ldots, x_s^n\right]$ and target node $\mathbf{x}_t = \left[x_t^1, x_t^2, \ldots, x_t^n\right]$. Applying the image technique in each dimension of the grid yields 2^n source nodes around the origin,

$$X_s = \begin{pmatrix} x_s^1, & x_s^2, & \ldots & x_s^n \\ x_s^1, & x_s^2, & \ldots & -x_s^n - 1 \\ \vdots & \vdots & \ddots & \vdots \\ x_s^1, & -x_s^2 - 1, & \ldots & x_s^n \\ -x_s^1 - 1, & x_s^2, & \ldots & x_s^n \\ \vdots & \vdots & \ddots & \vdots \\ -x_s^1 - 1, & -x_s^2 - 1, & \ldots & -x_s^n - 1 \end{pmatrix}. \quad (13)$$

Similarly, for the target node,

$$X_t = \begin{pmatrix} x_t^1, & x_t^2, & \ldots & x_t^n \\ x_t^1, & x_t^2, & \ldots & -x_t^n - 1 \\ \vdots & \vdots & \ddots & \vdots \\ x_t^1, & -x_t^2 - 1, & \ldots & x_t^n \\ -x_t^1 - 1, & x_t^2, & \ldots & x_t^n \\ \vdots & \vdots & \ddots & \vdots \\ -x_t^1 - 1, & -x_t^2 - 1, & \ldots & -x_t^n - 1 \end{pmatrix}. \quad (14)$$

Nodes in X_s and X_t are order sources since these nodes are closest to the origin. The higher order sources arise from translating the nodes in sets X_s and X_t along each dimension, yielding countably infinite sets,

$$X_s^{im} = \{\mathbf{x} + 2\mathbf{w} \circ \mathbf{a}; \mathbf{x} \in X_s, \mathbf{a} \in \mathbb{Z}^n\}, \quad (15)$$

$$X_t^{im} = \{\mathbf{x} + 2\mathbf{w} \circ \mathbf{a}; \mathbf{x} \in X_t, \mathbf{a} \in \mathbb{Z}^n\}, \quad (16)$$

where $\mathbf{w} \circ \mathbf{a}$ denotes the Hadamard (element-wise) vector product of vectors $\mathbf{w}$ and $\mathbf{a}$. The potential difference between nodes $\mathbf{x}_s$ and $\mathbf{x}_t$ is

$$V = \sum_{\mathbf{x} \in X_s^{im}} (\phi(\mathbf{x} - \mathbf{x}_s) - \phi(\mathbf{x} - \mathbf{x}_t)) + \sum_{\mathbf{x} \in X_t^{im}} (\phi(\mathbf{x} - \mathbf{x}_t) - \phi(\mathbf{x} - \mathbf{x}_s)). \quad (17)$$

Assume the effective resistance of an n-dimensional infinite grid is $\Omega_{(\mathbf{k},\mathbf{w})}(\mathbf{x})$, where $\mathbf{k}$ is the ratio of the unit resistance along each dimension to the unit resistance along the first dimension. The effective resistance of a finite mesh can be described as

$$\frac{R_{eff}}{r} = \sum_{\mathbf{x} \in X_s^{im}} (\Omega_{(\mathbf{k},\mathbf{w})}(\mathbf{x} - \mathbf{x}_s) - \Omega_{(\mathbf{k},\mathbf{w})}(\mathbf{x} - \mathbf{x}_t)) + \sum_{\mathbf{x} \in X_t^{im}} (\Omega_{(\mathbf{k},\mathbf{w})}(\mathbf{x} - \mathbf{x}_t) - \Omega_{(\mathbf{k},\mathbf{w})}(\mathbf{x} - \mathbf{x}_s)). \quad (18)$$

III. SIMPLIFICATION OF THE EFFECTIVE RESISTANCE EXPRESSIONS

Although the effective resistance is accurately determined with (7), (11), and (12), more computationally efficient equations are desirable. An efficient approximation of (9) is described in [21],

$$\hat{\Omega}^k(x, y) = \frac{\sqrt{k}}{4\pi}\left[\ln\left(x^2 + ky^2\right) + 2\ln(\pi) + \gamma\right] + \sum_{i=0}^{4} a_i k^i, \quad (19)$$

where $\gamma \approx 0.5772$ is the Euler-Mascheroni constant [12], and the coefficients a_i of the expression are listed in Table II.

The error of (19) as compared to (9) is shown in Fig. 10. Note that the error approaches zero for large x and y. At small values of x and y, the error dramatically increases, significantly affecting the accuracy of the effective resistance.

TABLE II
COEFFICIENTS FOR THE POLYNOMIAL APPROXIMATION OF J_3 (19) [21]

i \ Case	$1 \leq k \leq 5$	$5 \leq k \leq 50$
0	4.7480×10^{-2}	2.5590×10^{-2}
1	-5.9890×10^{-2}	-3.3560×10^{-2}
2	8.1530×10^{-4}	-1.0780×10^{-2}
3	-1.2740×10^{-5}	2.2600×10^{-3}
4	9.0920×10^{-8}	-1.6690×10^{-4}

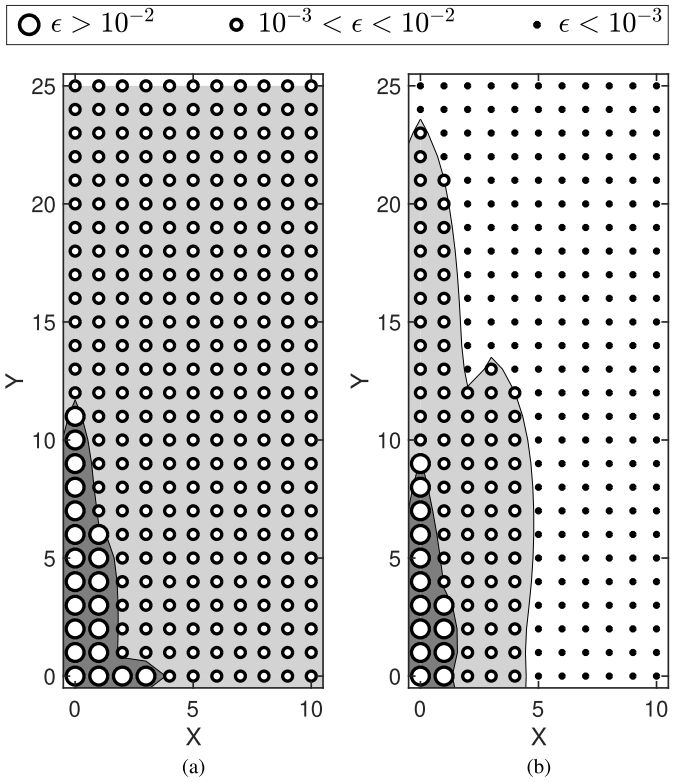

Fig. 10. Relative error ϵ between (9) and (19) for $0 \leq x \leq 10$, $0 \leq y \leq 25$, and $1 \leq k \leq 30$. a) Maximum error, and b) average error.

To alleviate this issue, the following function is proposed,

$$\Psi_{ij}^k(x, y) = \Psi^k(x + 2i w_x, y + 2j w_y) \tag{20}$$

$$\Psi^k(x, y) = \begin{cases} \Omega^k(x, y), & \text{if } \epsilon(x, y) > 10^{-2} \quad (21a) \\ \hat{\Omega}^k(x, y), & \text{otherwise;} \quad (21b) \end{cases}$$

where $\epsilon(x, y)$ is the relative error of (19) as compared to (9). Since $\Omega^k(x, y)$ only needs to be evaluated for a small subset of nodes where the error of (19) is large, the evaluation of $\Omega^k(x, y)$ can be replaced with a look-up table, providing an effective tradeoff between computational speed and accuracy.

Evaluation of the effective resistance in a finite mesh requires computing a double-infinite sum. The series in (12), however, quickly converges to 0. Using additional terms results in higher accuracy while requiring greater computational time. It is of interest to determine the optimal number of terms in series (12) to achieve acceptable accuracy in minimum time. Consider the following approximate equation for the effective resistance of a finite mesh,

$$\begin{aligned} R_{w_x, w_y}^{N,M} = \sum_{i=-N}^{N} \sum_{j=-M}^{M} \big(& 2\Omega_{ij}^k(x - x_0, y - y_0) \\ & + 2\Omega_{ij}^k(x - x_0, y + y_0 + 1) \\ & + 2\Omega_{ij}^k(x + x_0 + 1, y + y_0 + 1) \\ & + 2\Omega_{ij}^k(x + x_0 + 1, y - y_0) \\ & - \Omega_{ij}^k(2x_0 + 1, 0) - \Omega_{ij}^k(2x_0 + 1, 2y_0 + 1) \\ & - \Omega_{ij}^k(0, 2y_0 + 1)) - \Omega_{ij}^k(2x + 1, 0) \\ & - \Omega_{ij}^k(2x + 1, 2y + 1) - \Omega_{ij}^k(0, 2y + 1) \\ & - 2\Omega_{ij}^k(0, 0)\big), \end{aligned} \tag{22}$$

where $N, M \in \mathbb{N}_0$ are the number of iterations required to evaluate the effective resistance of a finite mesh. The accuracy of (22) is evaluated for an 11×11, 25×25, and 51×51 grid. The relative error of (22) is illustrated in Fig. 11. Observe that in all cases setting $N = K = 4$ is sufficient to achieve 0.3% accuracy. Note that due to the low error of (21) for small x and y, the error is smaller if the effective resistance is evaluated between nearby nodes.

IV. CASE STUDIES

The primary contribution of this paper is the efficient estimation of the effective resistance of a finite grid of arbitrary size, exhibiting constant complexity. The proposed framework is particularly suitable for circuit analysis techniques based on an effective resistance [2], [3]. In this section, three applications of the proposed framework are presented. In Section IV-A, a method accelerating the nodal analysis of a grid is presented. In Section IV-B, this method is applied to the analysis of a capacitive touch screen. In Section IV-C, a three-dimensional analysis of resistive substrate noise is described.

A. Mesh Reduction Based on Effective Resistance

The nodal analysis process can be significantly accelerated by applying these effective resistance techniques if the grid dimensions are large and the number of nodes of interest are small. Consider a large grid Γ with dimensions $N_x \times N_y$. Define the nodes of interest as a set,

$$S \equiv S_v \cup S_i \cup S_o, \tag{23}$$

where S_v and S_i are subsets of nodes connected to, respectively, the voltage sources and current sources, and S_o is a subset of other nodes of interest. If the number of nodes of interest $|S| = n$ is much smaller than the total number of nodes within the network $|\Gamma| = N$, the effective resistance technique can significantly accelerate the analysis of IR drops within a grid. The entire network Γ can be reduced to a smaller network Γ_S by preserving the pairwise effective conductance. The conductance matrix $G \in \mathbb{R}^{n \times n}$ of this reduced network is [22], [26]

$$G^\dagger = -\frac{1}{2}\Big(R_S - \frac{1}{n}\big(\mathbf{1}_{n,n} R_S + R_S \mathbf{1}_{n,n}\big) + \frac{1}{n^2} \mathbf{1}_{n,1} R_S \mathbf{1}_{1,n} \Big), \tag{24}$$

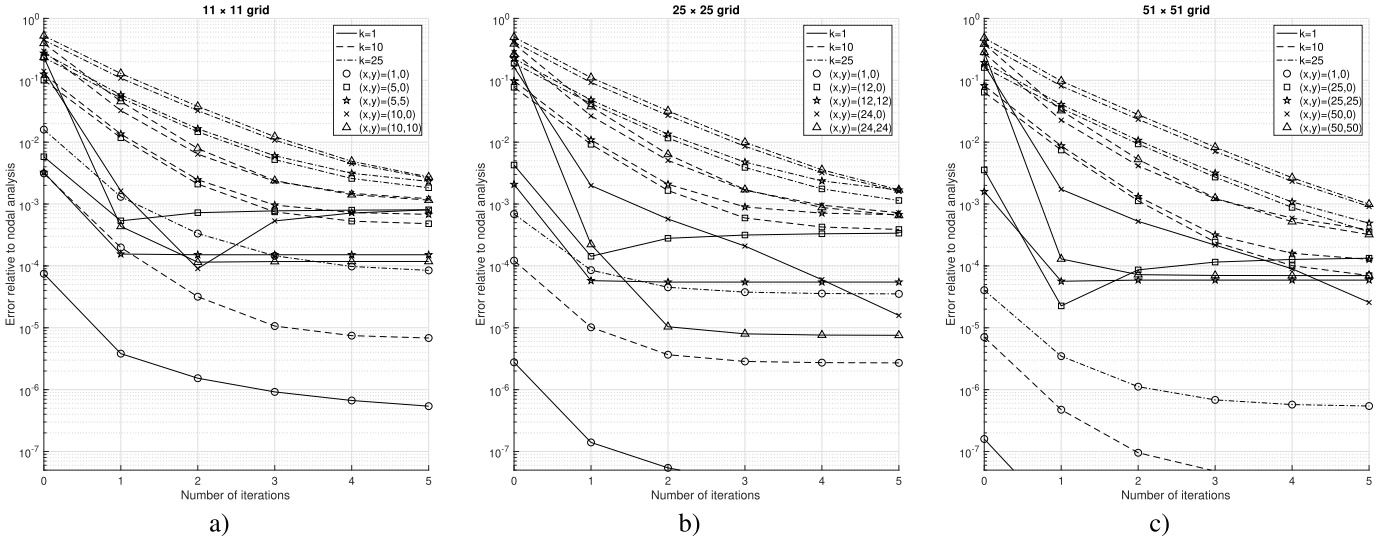

Fig. 11. Relative error of normalized effective resistance between $(0, 0)$ and (x, y) determined from (22) for $N = K \in [0, 5]$ as compared to a nodal analysis within a mesh with size a) 11×11, b) 25×25, and c) 51×51.

where $G^{\dagger}$ denotes the Moore-Penrose pseudoinverse of matrix G, $R_S \in \mathbb{R}_{\geq 0}^{n \times n}$ is the matrix of the effective resistance between each pair of nodes in S, and $\mathbf{1}_{a,b}$ is an $a \times b$ matrix with all entries equal to one. After the conductance matrix is recovered, the reduced network can be evaluated by solving the linear system,

$$\begin{bmatrix} G & B \\ B^T & \mathbf{0} \end{bmatrix} \begin{bmatrix} V \\ I \end{bmatrix} = \begin{bmatrix} J \\ F \end{bmatrix}, \tag{25}$$

where V and I are, respectively, the node voltages and currents through the voltage sources. B, J, and F encode the current and voltage sources.

The speed of (24) and (25) for estimating the effective resistance within a mesh is compared to nodal analysis using the Numpy and Scipy Python packages [27] on an eight core 3.40 GHz Intel Core i7-6700 machine with 24 GB RAM. The comparison is depicted in Fig. 12. Nodal analysis in circuits larger than 10^7 nodes could not be performed due to insufficient memory. Note that while the computational time of the nodal analysis process scales with grid size N, the computational time of the infinity mirror technique scales with the number of nodes of interest n. The bottom-right corner of the plot in Fig. 12a is the area where the grid size is large and the number of nodes of interest is small. The infinity mirror technique provides the largest speedup in this situation. In Fig. 12b, the relationship between the speedup due to (24) and (25) and the fraction of nodes of interest is presented. The results suggest that the framework provides significant computational speedup if finding the voltage at only 0.23% of the nodes is required (i.e., one in 430 nodes). For example, in a $10^3 \times 10^4$ grid, determining the voltage at 1,000 nodes using nodal analysis would require 3,430 seconds. Applying (24) and (25) results in a 17 fold speedup, requiring only 196 seconds to complete. If the number of nodes of interest is reduced to 100, the speedup reaches 1,400, completing in 2.37 seconds.

B. Resistive Noise in Capacitive Touch Screen

A possible application of the infinity mirror technique is the analysis of conductive media. An example of a conductive medium is a capacitive screen. The typical structure of a capacitive touch screen is shown in Fig. 13a [28]. An important component of the touch screen panel is the display cathode electrode providing a reference voltage for the screen. Resistive noise in the electrode layer of the display cathode may affect the accuracy of the touch recognition process. The accuracy of the touch sensor can therefore be enhanced by considering resistive noise during the sensor design process. An accurate estimate of the resistance typically requires significant computational time due to the finite element method extraction process often utilized for this task. The analysis can however be vastly accelerated by applying the infinity mirror technique to the equivalent model of the panel shown in Fig. 13b [28]. The method of mesh reduction presented in Section IV-A is utilized to accelerate this analysis process.

The results for evaluating the effective resistance for trace resistances of 0.1 Ω and 100 Ω are shown, respectively, in Figs. 13c and 13d. These results are consistent with the Q3D extraction process described in [28], significantly reducing the analysis time while maintaining the high accuracy of the effective resistance estimation.

C. Resistive Substrate Noise

A three-dimensional mesh is widely utilized to model conductive media, including thermal paths and substrate noise. Substrate noise is a common issue in mixed-signal VLSI circuits. While several advanced techniques for mitigation of substrate coupling exist, including guard rings and silicon-on-insulator technology [29], these techniques may significantly complicate the fabrication process. It is therefore necessary to estimate the magnitude of the substrate noise. The application of a three-dimensional network to substrate noise analysis is presented in this case study.

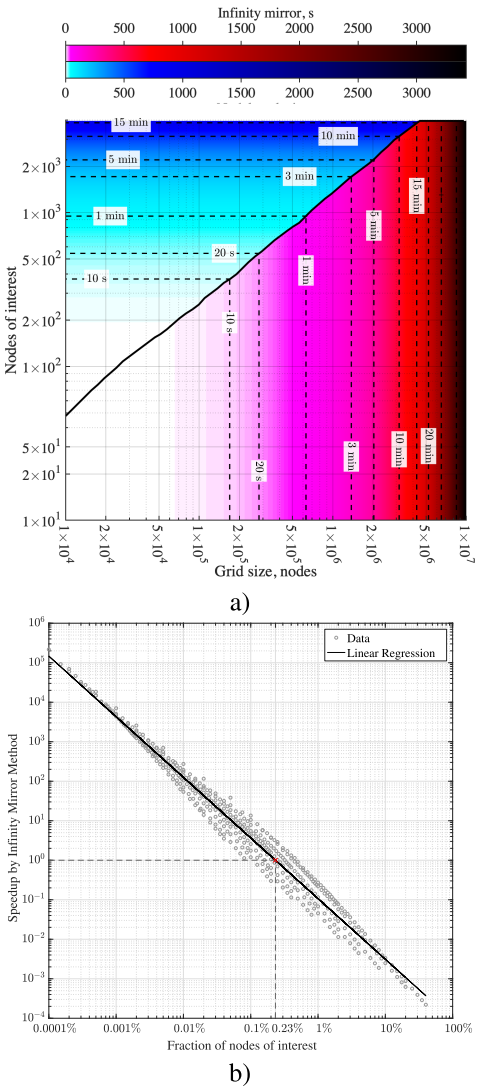

Fig. 12. Comparison of (24) and (25) to nodal analysis for $10 < n < 200$ and $10^4 < N < 10^7$. (a) Computational time (in seconds) to calculate the voltage at n nodes of interest in a grid with N nodes. The black line indicates n and N for which both techniques exhibit approximately equal time. (b) Speedup due to the use of (24) as compared to a pure nodal analysis as a function of $\frac{n}{N}$.

A frequent scenario in mixed-signal circuits is noise coupling between a digital aggressor and an analog victim. An equivalent circuit model of a mixed-signal circuit is shown in Fig. 14. The current I in the digital circuit would ideally flow into the digital ground. With substrate coupling, however, a sizable current flows into the analog ground, affecting the performance of the sensitive analog circuits.

The voltage v_{ga} at the analog ground terminal is

$$v_{ga} = \frac{I R_{ga} R_{gd}}{R_{gd} + R_s + R_{ga}}, \tag{26}$$

where R_{gd} and R_{ga} are, respectively, the resistance of the digital and analog ground distribution network, and R_s is the substrate resistance. Note that if the substrate resistance is large, the analog ground voltage converges to zero while reducing the substrate resistance, increasing the analog ground voltage.

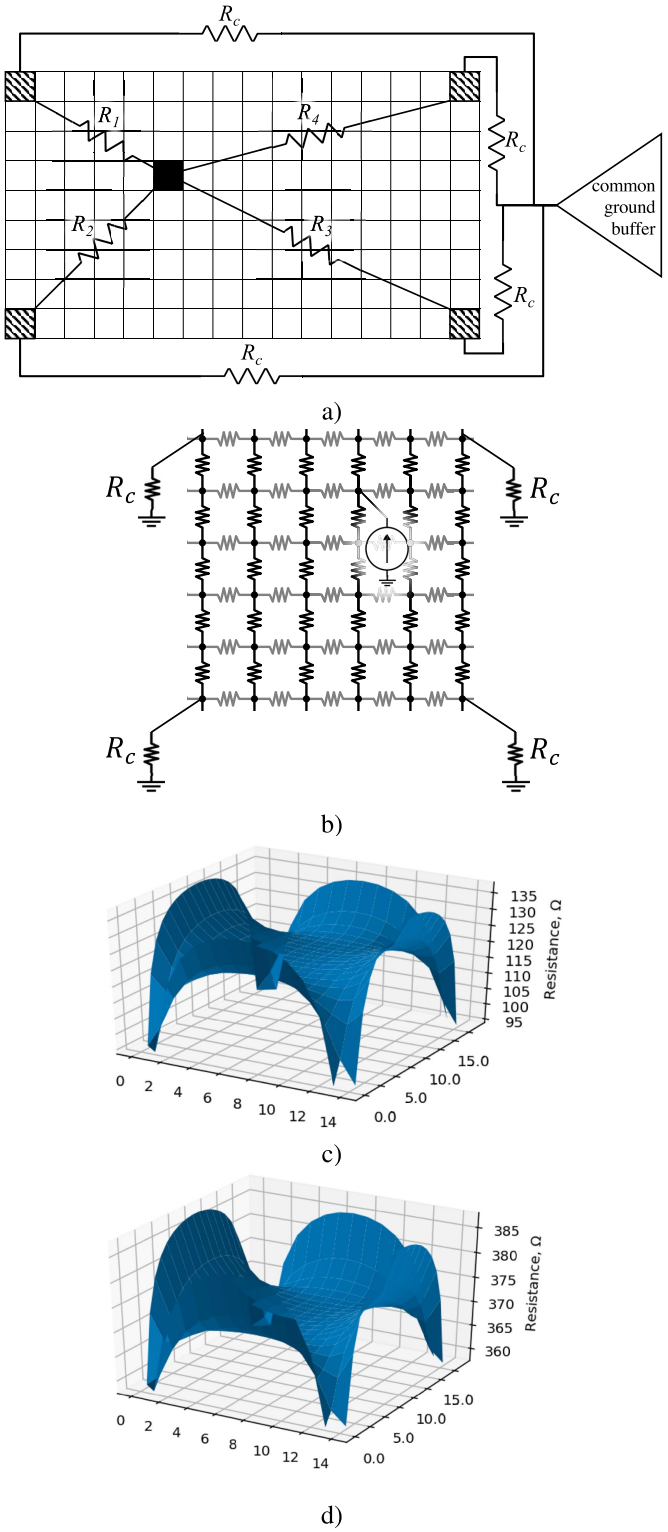

Fig. 13. Estimation of the effective resistance in a touch screen panel. a) Structure of the panel, b) equivalent circuit model, c) effective resistance with a 0.1 ohm trace resistance, and d) effective resistance with a 100 ohm trace resistance.

The infinity mirror technique can be used to evaluate the effective resistance between substrate contacts. Consider a

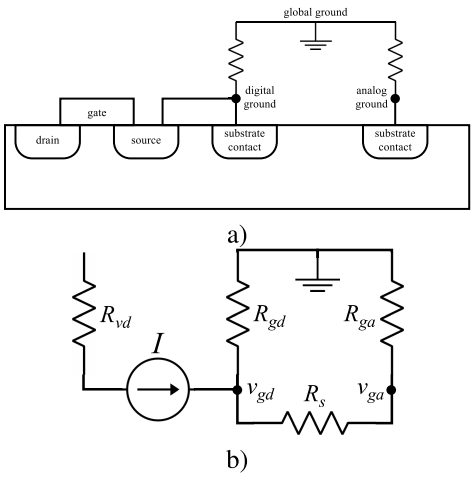

Fig. 14. Resistive substrate coupling mechanism in a mixed-signal complementary metal-oxide-semiconductor (CMOS) circuit. The substrate ground contacts for the analog and digital grounds are connected to the global ground through, respectively, an analog and digital ground distribution network. (a) Side view of the substrate, and (b) equivalent circuit model of the noise injection process.

TABLE III
PARAMETERS FOR SUBSTRATE NOISE EVALUATION

Parameter	Symbol	Value
Analog ground network resistance	R_{ga}	25 Ω
Digital ground network resistance	R_{gd}	25 Ω
Unit cell resistance	r_s	1 Ω
Digital circuit current	I	25 mA
Separation along y-dimension	y	0
Grid z-dimension parameter	w_z	10
Cell dimensions	dx,dy,dz	1 μm

uniform three-dimensional grid with unit resistance r_s, infinite x-y dimensions, and finite z-dimension w_z. The analog and digital substrate contacts are represented by two terminals on the top surface of the grid separated by an $(x, y, 0)$ vector. Applying (18) yields

$$R_s = 2r_s \sum_{p\in\mathbb{Z}} \Omega_{00p}(x, y, 0) + \Omega_{00p}(x, y, 1) - \Omega_{00p}(0, 0, 0) - \Omega_{00p}(0, 0, 1), \quad (27)$$

where

$$\Omega_{ijp}(x, y, z) = \Omega(x + 2w_x i, y + 2w_y j, z + 2w_z p). \quad (28)$$

Expression (27) is applied to (26) to determine the minimum distance between analog ground terminals. The parameters are listed in Table III. The resulting ground voltage is shown in Fig. 15. If the spacing is small, the substrate noise is significantly lower with increasing separation. After 20 μm, however, the space does not have a significant effect on the coupling noise. Note again that the analysis time is significantly reduced by avoiding a costly nodal analysis process [30]. The resistance measurement for each separation is completed on average in 2.76 seconds. A nodal analysis of a three-dimensional substrate with a size of 200 μm × 200 μm × 10 μm requires approximately 30.2 seconds, consistent with Fig. 12, indicating an approximate tenfold speedup.

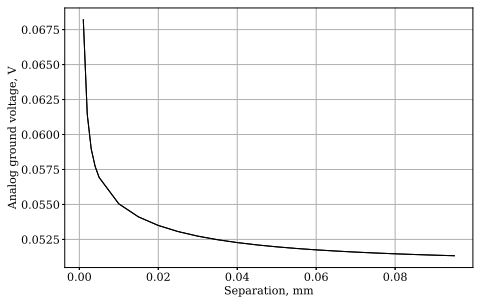

Fig. 15. Analog ground voltage as a function of the distance between the digital and analog ground terminals.

V. CONCLUSIONS

An infinity mirror technique is proposed here that maps a rectangular resistive grid structure with finite dimensions into an infinite grid. Extending the contributions in [21], where semi-infinite structures are considered, the methodology described here is applicable to those structures where one or both dimensions are finite. In addition, the framework is extended to higher dimensional topologies, evaluating the effective resistance in finite structures with three and more dimensions. The proposed expressions exhibit high accuracy and outperform the nodal analysis method in terms of computational speed. Using the infinity mirror technique, the effective resistance between two points in an anisotropic finite mesh can be determined within 1% accuracy. Several orders of magnitude speedup in IR drop analysis in large grids is achieved in case studies by utilizing closed-form expressions for the effective resistance. The most significant reduction in computational time is achieved in those cases where only a small fraction of nodes needs to be evaluated. These results can be beneficial to a variety of applications, including power grid and substrate analysis in VLSI circuits, estimation of commute times in random walks, and the analysis of isotropic and anisotropic conductive media [22]–[24], [31]–[34].

REFERENCES

[1] A. Ciprut, "Grids in very large scale integration systems," Ph.D. dissertation, Dept. Elect. Comput. Eng., Univ. Rochester, New York, NY, USA, May 2019.
[2] S. Köse and E. G. Friedman, "Efficient algorithms for fast IR drop analysis exploiting locality," *Integration*, vol. 45, no. 2, pp. 149–161, Mar. 2012.
[3] E. Liu and E. Li, "Fast voltage drop modeling of power grid with application to silicon interposer analysis," in *Proc. IEEE Electron. Compon. Technol. Conf.*, May 2013, pp. 1109–1114.
[4] M. Popovich, M. Sotman, A. Kolodny, and E. G. Friedman, "Effective radii of on-chip decoupling capacitors," *IEEE Trans. Very Large Scale Integr. (VLSI) Syst.*, vol. 16, no. 7, pp. 894–907, Jul. 2008.
[5] S. Zhao, K. Roy, and C.-K. Koh, "Decoupling capacitance allocation and its application to power-supply noise-aware floorplanning," *IEEE Trans. Comput.-Aided Design Integr. Circuits Syst.*, vol. 21, no. 1, pp. 81–92, Jan. 2002.
[6] A. Ghosh, S. Boyd, and A. Saberi, "Minimizing effective resistance of a graph," *SIAM Rev.*, vol. 50, no. 1, pp. 37–66, 2008.
[7] J. M. Kosterlitz and D. J. Thouless, "Ordering, metastability and phase transitions in two-dimensional systems," *J. Phys. C, Solid State Phys.*, vol. 6, no. 7, p. 1181, Apr. 1973.
[8] Y. Ogasahara, M. Hashimoto, T. Kanamoto, and T. Onoye, "Measurement of supply noise suppression by substrate and deep N-well in 90nm process," in *Proc. IEEE Asian Solid-State Circuits Conf.*, Nov. 2008, pp. 397–400.

[9] A. K. Chandra, P. Raghavan, W. L. Ruzzo, R. Smolensky, and P. Tiwari, "The electrical resistance of a graph captures its commute and cover times," *Comput. Complex.*, vol. 6, no. 4, pp. 312–340, 1996.
[10] A. H. Zemanian, "Infinite electrical networks: A reprise," *IEEE Trans. Circuits Syst.*, vol. 35, no. 11, pp. 1346–1358, Nov. 1988.
[11] R. E. Aitchison, "Resistance between adjacent points of Liebman mesh," *Amer. J. Phys.*, vol. 32, p. 566, Jul. 1964.
[12] W. H. McCrea and F. J. W. Whipple, "Random paths in two and three dimensions," *Proc. Roy. Soc. Edinburgh*, vol. 60, no. 3, pp. 281–298, Jan. 1940.
[13] B. van der Pol and H. Bremmer, *Operational Calculus Based on the Two-Sided Laplace Integral*. Cambridge, U.K.: Cambridge Univ. Press, 1950.
[14] G. Venezian, "On the resistance between two points on a grid," *Amer. J. Phys.*, vol. 62, no. 11, pp. 1000–1004, Nov. 1994.
[15] D. Atkinson and F. J. Van Steenwijk, "Infinite resistive lattices," *Amer. J. Phys.*, vol. 67, no. 6, pp. 486–492, Jun. 1999.
[16] K. Brown. *Infinite Grid of Resistors*. Accessed: Apr. 12, 2020. [Online]. Available: https://www.mathpages.com/home/kmath668/kmath668.htm
[17] J. Cserti, "Application of the lattice green's function for calculating the resistance of an infinite network of resistors," *Amer. J. Phys.*, vol. 68, no. 10, pp. 896–906, Oct. 2000.
[18] P. G. Doyle and J. L. Snell, *Random Walks and Electric Networks*, vol. 22. Washington, DC, USA: Mathematical Association of America, 1984.
[19] M. Jeng, "Random walks and effective resistances on toroidal and cylindrical grids," *Amer. J. Phys.*, vol. 68, no. 1, pp. 37–40, Jan. 2000.
[20] S. Köse and E. G. Friedman, "Effective resistance of a two layer mesh," *IEEE Trans. Circuits Syst. II, Exp. Briefs*, vol. 58, no. 11, pp. 739–743, Nov. 2011.
[21] R. Bairamkulov and E. G. Friedman, "Effective resistance of two-dimensional truncated infinite mesh structures," *IEEE Trans. Circuits Syst. I, Reg. Papers*, vol. 66, no. 11, pp. 4368–4376, Nov. 2019.
[22] A. Carmona, A. M. Encinas, and M. Mitjana, "Kirchhoff index of periodic linear chains," *J. Math. Chem.*, vol. 53, no. 5, pp. 1195–1206, May 2015.
[23] H. Zhang and Y. Yang, "Resistance distance and kirchhoff index in circulant graphs," *Int. J. Quantum Chem.*, vol. 107, no. 2, pp. 330–339, Nov. 2007.
[24] F.-Y. Wu, "Theory of resistor networks: The two-point resistance," *J. Phys. A, Math. Gen.*, vol. 37, no. 26, pp. 6653–6673, Jul. 2004.
[25] R. Jakushokas and E. G. Friedman, "Power network optimization based on link breaking methodology," *IEEE Trans. Very Large Scale Integr. (VLSI) Syst.*, vol. 21, no. 5, pp. 983–987, May 2013.
[26] F. Dörfler and F. Bullo, "Kron reduction of graphs with applications to electrical networks," *IEEE Trans. Circuits Syst. I, Reg. Papers*, vol. 60, no. 1, pp. 150–163, Jan. 2013.
[27] (2019). *SciPy: Reference Guide*. Accessed: Apr. 12, 2020. [Online]. Available: https://docs.scipy.org/doc/scipy/scipy-ref-1.4.1.pdf
[28] C.-J. Lee, J. K. Park, S. Kim, and J.-H. Chun, "A study on a lattice resistance mesh model of display cathode electrodes for capacitive touch screen panel sensors," *Procedia Eng.*, vol. 168, pp. 884–887, Sep. 2016.
[29] R. M. Secareanu *et al.*, "Substrate coupling in digital circuits in mixed-signal smart-power systems," *IEEE Trans. Very Large Scale Integr. (VLSI) Syst.*, vol. 12, no. 1, pp. 67–78, Jan. 2004.
[30] E. Salman and E. G. Friedman, *High Performance Integrated Circuit Design*. New York, NY, USA: McGraw-Hill, 2012.
[31] J. Xie, Y. Jia, and M. Miao, "High sensitivity knitted fabric bi-directional pressure sensor based on conductive blended yarn," *Smart Mater. Struct.*, vol. 28, no. 3, Feb. 2019, Art. no. 035017.
[32] J. Xie and H. Long, "Equivalent resistance calculation of knitting sensor under strip biaxial elongation," *Sens. Actuators A, Phys.*, vol. 220, pp. 118–125, Dec. 2014.
[33] E. Bendito, A. Carmona, A. M. Encinas, and J. M. Gesto, "Characterization of symmetric M-matrices as resistive inverses," *Linear Algebra Appl.*, vol. 430, no. 4, pp. 1336–1349, Feb. 2009.
[34] S. J. Kirkland and M. Neumann, "The M-matrix group generalized inverse problem for weighted trees," *SIAM J. Matrix Anal. Appl.*, vol. 19, pp. 226–234, Jan. 1998.